LRIG3 IS REQUIRED IN RECOVERY FROM ACUTE INFLAMMATORY ASSAULT

by

KEVIN THOMAS MUELLER

A THESIS

Presented to the Department of Biology
and the Robert D. Clark Honors College
in partial fulfillment of the requirements for the degree of
Bachelor of Science

May 2023

An Abstract of the Thesis of

Kevin Mueller for the degree of Bachelor of Science
in the Department of Biology to be taken June 2023

Title: *Lrig3* is Required in Recovery from Acute Inflammatory Assault

Approved: *Annie Zemper Ph.D.*
Primary Thesis Advisor

Background and Aim. The mouse colon contains a suite of genes that provide a framework from which the structure and function of the colon is tightly regulated. The colon contains crypts: small, U-shaped invaginations in the epithelial layer that absorb water and secrete mucus. A gene from this suite of regulatory genes is called *Leucine-rich repeats and immunoglobulin-like domains 3 (Lrig3),* may regulate the size and structure of a specialized region of the colonic crypts. In homeostasis, *Lrig3*$^{-/-}$ mice have longer colons, taller crypts, more cells per crypt, and more stem and progenitor cells than wildtype (*WT*) mice. This indicates that *Lrig3* is required for restricting the size of the stem cell niche. It is unknown if these abnormalities perturb the regenerative capabilities of the colon. The aim of my study was to test the hypothesis that loss of *Lrig3* impairs colonic regeneration after acute inflammatory assault.

Method. To address our study aims, we administered *WT* (B6, n=4) and *Lrig3*$^{-/-}$ mice (n=4) 3% Dextran Sodium Sulfate (DSS) in drinking water for seven days to cause crypt destruction and local inflammation. We initially sought to examine crypt regeneration over the subsequent seven days, but the *Lrig3*$^{-/-}$ mice lost >20% of their body weight and the study had to be halted 24 hours after resumption of normal drinking water, due to this extreme and unexpected weight loss. We then sacrificed all

mice in both cohorts at this time, extracted the colons and performed anatomical, morphometric, protein expression, and analysis for genes associated with crypt structure and regeneration.

Results. *Lrig3*$^{-/-}$ mice displayed a higher susceptibility to DSS treatment than *WT* as supported by greater weight loss and increased colon shortening. Compared to *WT* mice, *Lrig3*$^{-/-}$ mice expressed lower levels of Ki-67+ cells/epithelial area (p=0.045). *Lrig3*$^{-/-}$ mice also had decreased Lrig1-positive cells per crypt (p<0.01). Cell death analysis revealed a greater number of TUNEL-positive cells in the base of the crypt of *Lrig3*$^{-/-}$ mice (p<0.01). Immunofluorescent analysis for markers of both secretory and absorptive epithelial cell lineages was not significantly different between genotypes after acute inflammatory assault. Finally, we found key receptor kinase signaling pathways were not aberrantly regulated at 24 hours after the DSS time course. (All statistical tests were a two-tailed student's t-test assuming unequal variance).

Conclusion. My study has determined that loss of *Lrig3* significantly impairs colonic regeneration after acute inflammatory assault. While the role of Lrig3 in colon homeostasis is still under investigation, Lrig3 protein plays a key role in colonic regeneration after injury, yet the mechanism of action remains unknown.

Acknowledgements

I would like to thank my primary advisor, Dr. Annie Zemper, and graduate mentor, Dr. Janelle Stevenson, for allowing me to contribute to this project and guiding me over the past 4 years. I am grateful for the opportunity I have been afforded in this lab to develop as a scientist and communicator. I wish to extend gratitude to Dr. Daphne Gallagher, my advisor for the entirety of my undergraduate experience and Clark Honors College representative on this thesis. I have enjoyed the hours we have spent discussing everything from academic scheduling to the interesting collections available in European museums. Sincerest thanks to Dr. Daniel Grimes for his time and effort spent representing the Department of Biology on my committee and assisting my navigation through the departmental thesis process. Finally, I would like to thank my parents, Jeanne and Glen Mueller, who made my memorable experiences and education at the University of Oregon and the Clark Honors College possible. Without their continued support and willingness to send their son across the country for college I would not have been able to explore this beautiful state or take advantages of the opportunities this university has to offer.

Table of Contents

Introduction 8
Methods 18
Results 25
DSS-treated *Lrig3*$^{-/-}$ mice exhibit fewer proliferating cells than their *WT* counterparts. 26
TUNEL identifies more cells marked for programmed death in *Lrig3*$^{-/-}$ mice....27
DSS treated *Lrig3*$^{-/-}$ mice exhibit lower expression of Lrig1 than their *WT* counterparts 29
Regulation of differentiated cells is unchanged in *Lrig3*$^{-/-}$ mice after acute inflammatory assault. 32
Receptor kinase signaling is unchanged in DSS-treated *Lrig3*$^{-/-}$ mice 34
Discussion....36
Bibliography 42

List of Figures

Figure A.1 Cross Section of a Crypt of Lieberkühn. 9

Figure A.2: Typical endoscopic features of Ulcerative Colitis. 13

Figure A.3: Typical endoscopic features of Crohn's Disease. 14

Figure 1: DSS treated *Lrig3*$^{-/-}$ mice have fewer nuclei per crypt than *WT* mice. 26

Figure 2: DSS treated *Lrig3*$^{-/-}$ mice have fewer proliferating cells than their *WT* counterparts. 28

Figure 3: TUNEL identifies more cells marked for programmed death in *Lrig3*$^{-/-}$ mice. 30

Figure 4: DSS treated *Lrig3*$^{-/-}$ mice exhibit lower expression of Lrig1 than their WT counterparts. 31

Figure 5: Regulation of differentiated cells is unchanged in *Lrig3*$^{-/-}$ mice after acute inflammatory assault. 33

Figure 6: Receptor kinase signaling is unchanged in *Lrig3*$^{-/-}$ mice compared to *WT* mice. 35

List of Tables

Table 1: Chemical and Biological Reagents 22

Introduction

The mammalian colon has been shaped by millennia of evolution into a highly proliferative organ with a structure designed specifically to secrete mucus and absorb nutrients. The organ must serve as a protective barrier between the external environment and the internal organs while simultaneously facilitating the specific and penetrative absorption of crucial nutrients. A broad range of simple, columnar epithelial cells line the colon and provide these functions. These epithelial cells include various cell types maintained by a plethora of signals and cellular polarity. The epithelial cells lining the colon are organized into millions of small, U-shaped invaginations called the Crypts of Lieberkühn (Gordon Betts et al., 2022;"crypts") which are responsible for carrying out the functions of the colon. The cellular populations in the crypts undergo rapid replenishment driven by specialized stem cells residing in the base of each crypt structure (Figure A.1). The structure and functions of the colon are thus effectively maintained by the stem cells. To study the functions of this stem cell population efficiently, simpler, non-human models are frequently used. The murine colon, which is the animal model of this thesis, sheds its epithelial lining every 3-5 days and is strikingly homologous to the human colon (Gehart & Clevers, 2018). The human and murine colons are in fact so homologous that human tissue can be grafted to murine tissue and grown *in vivo* (Sugimoto et al., 2018). Such an effective model allows for close approximations of cell and protein responsibilities in both homeostasis and inflammatory states.

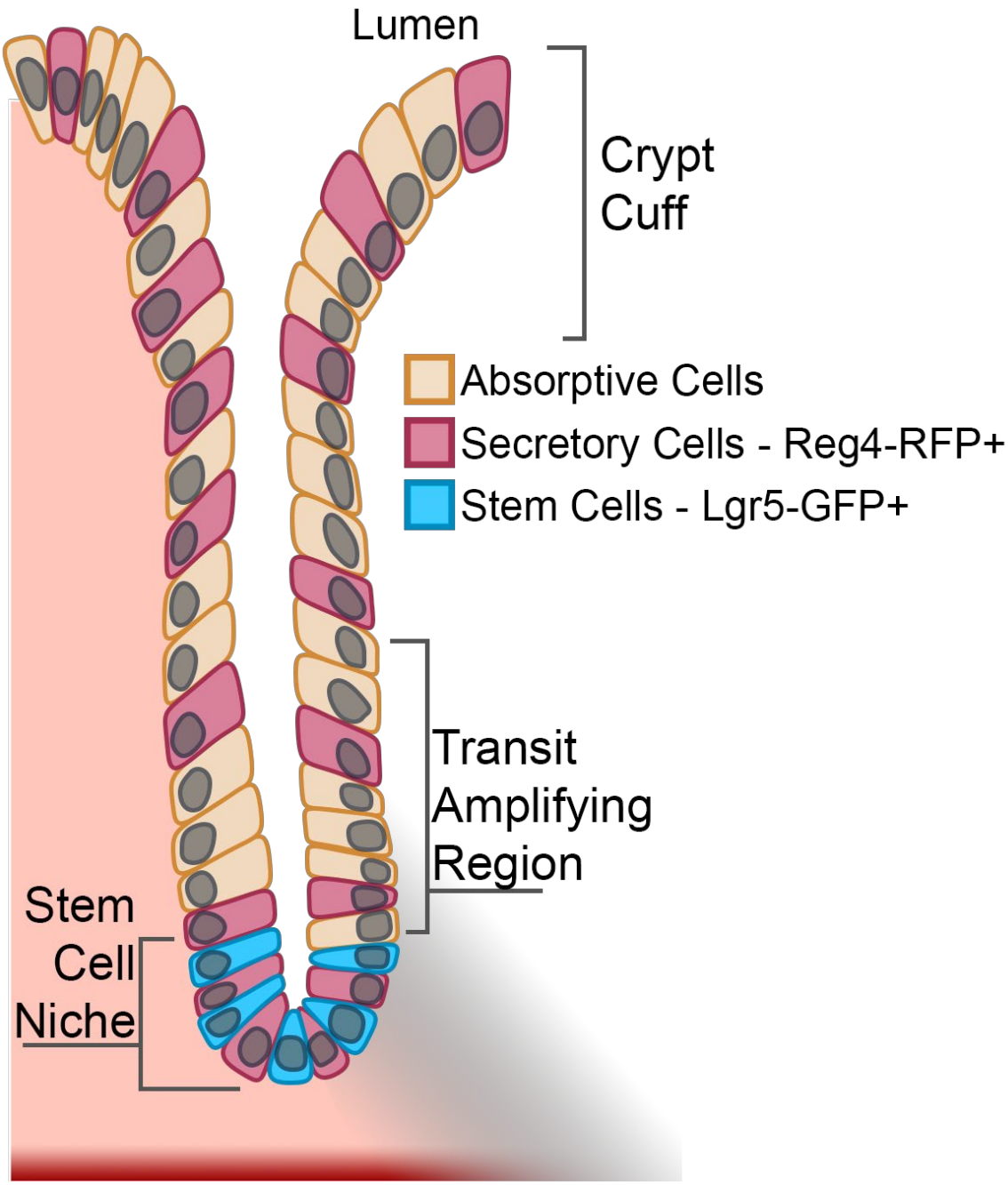

Figure A.1 Cross Section of a Crypt of Lieberkühn.

Crypts appear U-shaped when sliced longitudinally and display a stereotyped architecture with three distinct regions, a basal stem cell niche, a central transit amplifying region, and a final differentiated region spilling up against the lumen. Used with permission from Timothy W. Wheeler.

In the appropriate response to inflammation there is a renewal of epithelial tissue which enables recovery of homeostasis. This renewal is driven by the division of stem cells at the base of each crypt (Gehart & Clevers, 2018). Each colonic crypt is comprised of three main regions that each contribute to the overall functionality of the organ. The region at the base of the crypt, the stem cell compartment, or stem cell niche, consists of two distinct cell types: somatic stem cells and differentiated secretory cells (Figure A.1). The stem cells are commonly identified by expression of numerous proteins including Leucine-rich repeat-containing G-protein coupled receptor 5 (Lgr5) and Leucine-rich repeat immunoglobulin-like domains 1 (Lrig1) in homeostatic tissue. In addition to stem cells residing in the base of these epithelial crypts, intercalating with these crypt-base cells are cells called Deep Crypt Secretory Cells. These cells express Regenerating family marker 4 (Reg4) (Sasaki et al., 2016) and their function is to support the existing stem cell population, allowing those cells to properly function. When those stem cells in the colonic crypt do divide, some of their progeny migrate up into the transit amplifying (TA) region (Figure A.1).

The TA region is marked by highly proliferative cells that express the cell cycle marker Kiel-67 (Ki-67). This compartment is where most cellular division occurs and is crucial in regeneration following perturbations of the colon (Biressi et al., 2020). The TA region is also identified by the commitment of semi-differentiated cells to one of a few cellular fates. These fully committed cells complete their migration to the upper portion of the crypt, which is referred to as the “cuff” (Figure A.1). In their differentiated state, these cells are responsible for performing the critical functions of

the colon. The differentiated cellular population is predominantly composed of secretory and absorptive lineage cells (Biressi et al., 2020). Once cells reach the lumen at the top of the cuff, they undergo programmed cell death (Dufourt et al., 2004). Cell death is an important regulatory process here as if cell death did not occur while proliferation was maintained, these cells would choke the supply of precious resources to the burgeoning cells at the base of these epithelial crypts. This would prevent regeneration by crowding out new, immature cells.

While the cell signaling pathways which regulate the colonic epithelium are remarkably intricate and capable, they are not infallible. Failure of these mechanisms to properly regulate tissue regeneration can lead to a variety of diseases (Pérez et al., 2018). Colonic diseases frequently involve damage to the protective barrier preventing the internal environment of the body from directly contacting the lumen. In humans, degradation of this crucial lining can result in inflammation, infection, and even cancer formation (Vancamelbeke & Vermeire, 2017). The diseases resulting in acute and chronic inflammation are incompletely understood and significantly impact both physical and mental health (Pulley et al., 2020; Rawla et al., 2019).

There is one family of inflammatory diseases affecting humans that cannot easily be predicted and does not have a clear, definite etiology. These diseases fit into the category of Inflammatory Bowel Disease (IBD) and are characterized by improper functioning of the protective lining leading to bacterial infestation and destruction of crypts in damaged areas (Seyedian et al., 2019). One such disease, Ulcerative Colitis (UC), was estimated to affect nearly 600,000 Americans in 2009 and has been steadily increasing (Kappelman et al., 2013). Acute manifestations of this chronic disease are

defined by painful bouts of gut inflammation, which can generate large ulcers that typically resolve over days to weeks. The resolution of these acute bouts involves the reduction of inflammation and crypt regeneration (Seyedian et al., 2019).Without proper maintenance of the colon's protective barrier, patients are at heightened risk of frequent bouts with inflammatory diseases and related quality of life impairment (Pulley et al., 2020). Patients with UC present with complaints of stool frequency, rectal bleeding, and mucous discharge from the rectum (Seyedian et al., 2019). Additionally, all patients with IBD have a higher chance of being diagnosed with depression and anxiety (Mikocka-Walus et al., 2016). Clinically, patients with undiagnosed UC have a characteristic presentation remarkably like those with another form of IBD called Crohn's Disease. While UC consists of uninterrupted mucosal and submucosal ulcerations of the colon, Crohn's Disease is described as patchy with interruptions to ulcerations. Both forms of IBD can be difficult to diagnose without the use of colonoscopy techniques. As seen in Figures A.1 and A.2, the diseases are easily differentiable with colonoscopy procedures. Crohn's has a classic cobblestone appearance while UC appears more edematous and erythematous (Lee & Lee, 2016). Once the disease is identified, clinical treatments can be started and/or adjusted to the severity of the patient's disease. Unfortunately, clinical treatment is lifelong and is currently targeted towards symptomatology as opposed to the causative factors of the disease. Further research is required to identify the physiological origins of IBD, the impact of the inflammation on the colon lining, and for finding effective preventative measures and curative treatments.

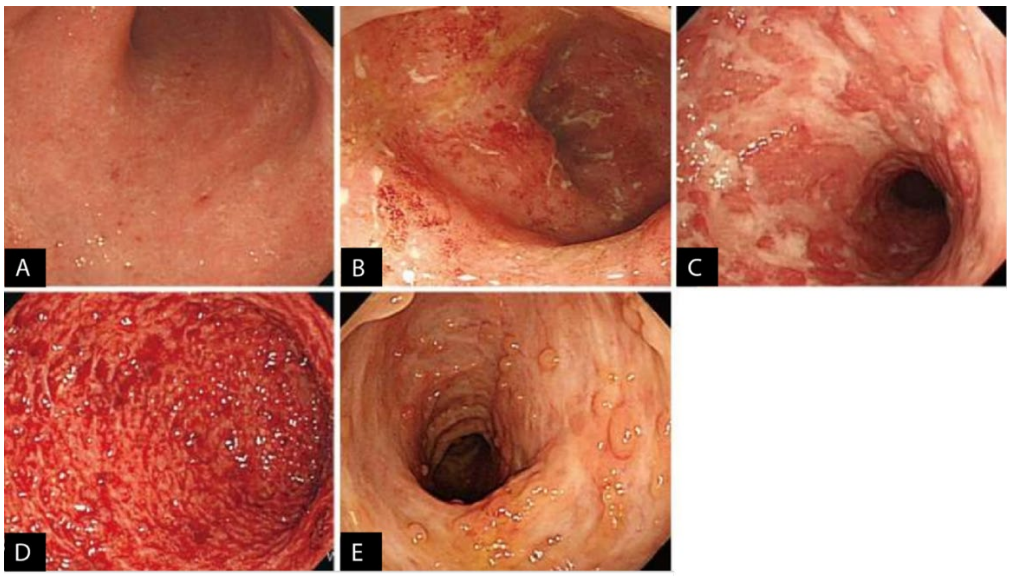

Figure A.2: Typical endoscopic features of Ulcerative Colitis.

(A) Mild: mucosal erythema, fine granularity, decreased vascular marking. (B) Moderate: marked erythema, loss of vascular marking, erosions. (C) Severe: ulcers. (D) Severe: spontaneous bleeding. (E) Luminal narrowing with pseudopolyps. Adapted from Lee & Lee 2016, an Open Access article distributed under the terms of the Creative Commons Attribution Non-Commercial License (http://creativecommons.org/licenses/by-nc/3.0/) which permits unrestricted non-commercial use, distribution, and reproduction in any medium.

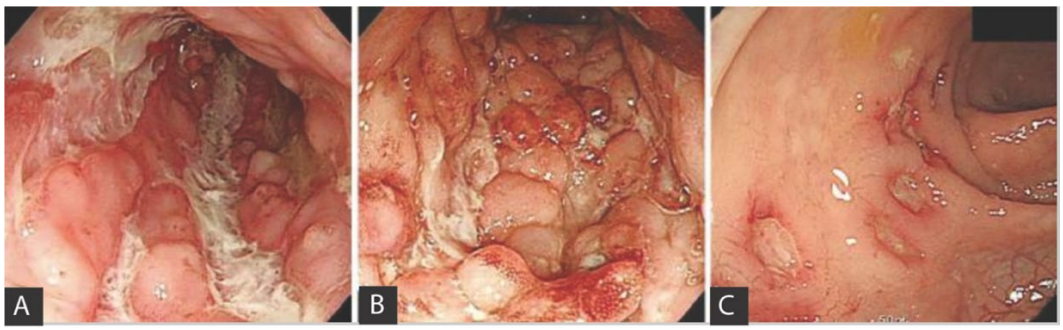

Figure A.3: Typical endoscopic features of Crohn's Disease.

(A) Longitudinal ulcers. (B) Cobblestone appearance. (C) Aphthous ulcers showing longitudinal array. Adapted from Lee & Lee 2016, an Open Access article distributed under the terms of the Creative Commons Attribution Non-Commercial License (http://creativecommons.org/licenses/by-nc/3.0/) which permits unrestricted non-commercial use, distribution, and reproduction in any medium.

My thesis uses a mouse IBD model which provides insight into the greater functionality of the colon after acute inflammation. The study I conducted uses a loss-of-function genetic approach and combines that with the IBD model. These studies categorized as 'basic science' but have clinical relevance (Wray et al., 2021). The reality of current treatment for IBD is that it does not address or include normalization of intestinal cellular functions at the molecular level (Boye et al., 2022). Studies like my own describe the phenotype of genetic susceptibility, which is an asset to medical researchers identifying viable treatment options for the predisposed.

Previously, I discussed the lack of a definitive etiology of these diseases. While there is no complete etiology, the generally accepted hypothesis is that these diseases arise as an aggressive and inappropriate inflammatory response to environmental triggers within patients who are in some way genetically predisposed to IBD (Qin, 2012). There exists a wide variety of research studies that have investigated the etiology and underlying mechanism of IBD pathogenesis (Coskun et al., 2013). These have been invaluable to the understanding of and subsequent development of Janus Kinase inhibitor treatments for these conditions, yet these drugs predominantly treat the symptoms and not the underlying disease cause. In addition, current biologic therapies are not universal and do little to improve the rates of emergent colectomy (Aslam et al., 2022; Worley et al., 2021). Emergent colectomy is a surgical removal of the colon in patients with acute severe ulcerative colitis that cannot be reversed, unlike starting a new biological therapy (De Simone et al., 2021). Beyond treatments, our understanding of the recovery from these inflammatory injury conditions is limited. One of the key areas that lacks data is our grasp of the molecular mechanisms responsible for

rebuilding the morphology of the colon from disease states after acute stress and injury. My thesis work contributes to this area of research.

In my studies, I tested mice lacking the ability to produce a gene, *Leucine-rich repeats and immunoglobulin-like domains 3* (*Lrig3*), and how these mice respond to acute inflammatory assault. Lrig3 is a member of a protein family that interacts with ErbB (epidermal growth factor) and epidermal growth factor receptor (EGFR) signaling (Abraira et al., 2010). More specifically Lrig3 has been shown to occupy diverse roles across tissues, in some cases stabilizing the ErbB family and opposing the degrative action of its founding familial gene, *Lrig1*, (Rafidi et al., 2013) but in other cases acting independently to the degree that it is required, such as in the formation of the neural crest in frogs (Zhao et al., 2008). The mammalian Lrig family occupies many molecular roles across various organisms, yet little is known about the function of Lrig3 (Simion et al., 2014). In previous studies, *Lrig3*$^{-/-}$ mice have been shown to lack a proper tissue morphometric profile, as they have more cells per crypt, greater musical area, and longer colons than *WT* mice (Stevenson et al., 2022 In Revision). Additionally, these mice have more stem and progenitor cells than their *WT* counterparts.

In other organ systems, *Lrig3* functions in various molecular roles. In the inner ear, *Lrig3* acts redundantly of its familial gene *Lrig1* (del Rio et al., 2013) in the otic epithelium to control inner ear morphogenesis. A few years after the publication of that study, another team of researchers found *Lrig3* acts as a potent tumor suppressor against the invasion of glioblastoma cells. In addition to this function, *Lrig3* was critical in modulating apoptosis and proliferation (Guo et al., 2015). This study found *Lrig3* to be a positive regulator of cell death, and negative regulator of the EGFR signaling

pathway. A third study found the actions of an *Lrig3* family member, Lrig1, to be opposed by Lrig3 in cell culture, which identified a unique role for Lrig3 despite its structural homology to Lrig1 (Rafidi et al., 2013). In the intestine, Lrig1 is a marker of stem cells that are non-cycling and long lived. Intestinal Lrig1^{+} cells exhibit upregulation of genes involved in cell cycle repression and response to oxidative damage (Powell et al., 2012). The inappropriate cellular census observed in *Lrig3*$^{-/-}$ mice in homeostasis indicates that the function of *Lrig3* is not redundant of *Lrig1* (Stevenson et al., 2022 In Revision) in the colon. In alignment with these observations, I hypothesize *Lrig3* is required for proper colonic regeneration following acute inflammatory assault. My studies examine the molecular profile behind IBD in *Lrig3*$^{-/-}$ mice and demonstrate the necessity of *Lrig3* in the preservation of a stem cell niche during colonic regeneration.

Methods

All biological reagents are listed in table 1 below.

Mouse Husbandry

C57bl/6 and *Lrig3* mice were housed in a pathogen-free, light cycle-controlled environment. Mice were fed standard chow and provided water ad libitum. All performed mice procedures were approved by the University of Oregon Institutional Animal Care and Use Committee (IACUC). All mice entered the Dextran Sodium Sulfate (DSS) time-course between the ages of six-eight weeks. 12 mice total, six per genotype, were involved in the experiment. All mice were sacrificed by cervical dislocation. At time of sacrifice, colons were removed and flushed with ice-cold Phosphate Buffered Saline (PBS). The length of each colon was measured with a ruler before bifurcation.

Dextran Sodium Sulfate (DSS) Course

DSS solution was made by measuring the appropriate amount of DSS to make a three percent by mass solution. This was dissolved in acidified drinking water and distributed ad libitum to mice for six days. DSS water was replaced with regular drinking water after six days and mice were allowed to recover on untreated water for 24 hours.

Image Acquisition and Preparation

All images were obtained using a Nikon Eclipse/Ds-Ri2. Nuclei per crypt were quantified using five minute 4',6-diamidino-2-phenylindole (DAPI). Most markers were quantified on the number of positive cells per crypt/animal with a few exceptions. Lrig1 was quantified as a measure of highest Lrig1+ expressing cell from the base of the crypt against the length of the entire crypt. These data were generated using the Nikon NIS-Elements measurement tool. Epithelial area was measured as an outline of intact crypts (Figure 2A).

In preparation for presentation of images, ".nd2" files generated by Nikon NIS-Elements were exported as ".tif" files. ".tif"s were imported to Adobe Photoshop where each monochannel was assigned either magenta or green.

Blinding and Statistical Analysis

Slides are blinded before imaging and remain blind until quantification was completed. After imaging, images are run through an R program written by Dr. Timothy W. Wheeler that assigns randomized names to images. The files generated by this program are the images upon which quantification is completed. Data collected from these images are analyzed using the analysis tool Pak in Microsoft Excel. Epithelial area was calculated by outlining mostly intact crypts as a region of interest (ROI) file. These ROIs were processed with an ImageJ macro measuring the area in pixels which was later converted to microns from conversion factors collected in imaging. Student's two-tailed T-test, assuming unequal variance, was run across animals' average scores for the measured variable. The n for each stain is reported in the associated figure.

Tissue Preparation

Tissue for frozen sections was pinned to wax surface and fixed using four percent paraformaldehyde for one hour on a shaker. This tissue was then subject to three concatenated five minute washes in PBS. These blocks were then submerged in 30% sucrose in PBS overnight at four degrees Celsius. Tissue was removed from the four degree Celsius bath and embedded in optimal cutting temperature tissue compound for sectioning. All slides were cut in 10μm sections with a Leica cryostat and stained according to protocols stated below.

Receptor Tyrosine Kinase (RTK) Array

Lysates were prepared by diluting protein in a Laemmli buffer and boiling in five percent β-mercaptoethanol at 95˚C for five minutes. Each array membrane (see table below for kit information) was added to the multi-well dish blocked in Array Buffer one for one hour at room temperature on a shaker. Lysates were diluted with Array Buffer one to a final volume of 1.5 mL. Array buffer 1 was removed from the membranes and lysate dilutions were added then incubated overnight at four degrees Celsius on a shaker. Arrays were passed through three 10-minute washes in Wash Buffer on a shaker. Anti-Phospho-Tyrosine-HRP Detection Antibody was diluted in Wash Buffer and added to the well dishes. Arrays were returned to the dishes, covered, and incubated for two hours on a shaker at room temperature. Arrays were passed through three 10-minute washes in Wash Buffer on a shaker. Each array was incubated for one minute with Chemi Reagent mix, then membranes were wrapped in plastic wrap. Chemifluorescent images of the membranes were obtained with a GE Healthcare Amersham Typhoon.

Immunohistochemistry (IHC) staining

Frozen tissue slides were removed from the -80˚C freezer and allowed to thaw for 15 minutes. Following warming to room temperature, slides were washed in PBS three times for three minutes each. Following washes, a PAP pen was used to create hydrophobic barriers around the tissue contained on each slide. Tissue was incubated in 0.3% triton X-100, one percent Bovine Serum Albumin (BSA) Blocking Buffer for one hour at room temperature (RT). Following incubation, 100µl of primary antibody in antibody-specific dilutions in Blocking Buffer ranging from 1:100-1:750 were pipetted onto experimental slides and incubated overnight at 4˚C. Secondary only slides were incubated in Blocking Buffer overnight instead of receiving primary antibody dilutions. Slides were again passed through three PBS washes for three minutes each. A fluorescently tagged secondary antibody was diluted on the order of 1:500 in blocking buffer and added in 100µl aliquots to all slides. Slides were incubated for one hour at RT before being passed through three concatenated washes, first a three minute PBS wash, then a DAPI wash, and finally a minute PBS wash. The DAPI wash consisted of a 1:10,000 dilution of DAPI in PBS. Following the third wash, slides were cover-slipped with n-propyl gallate used as the mounting agent. Slides were stored at four degrees Celsius before imaging. Ki-67 antibody staining followed the same protocols except for the overnight incubation period with the primary antibody, which was at room temperature, not four degrees Celsius.

Terminal deoxynucleotidyl transferase dUTP nick end labeling (TUNEL)

Frozen tissue slides were removed from the -80˚C freezer and allowed to thaw for 15 minutes. Slides were rinsed in two PBS washes for three minutes each and then permeabilized. Permeabilization consisted of a one-minute incubation with 20˚C 0.1% Triton X-100. Following this incubation slides were washed in PBS two times for three minutes each. 50µl TUNEL mix was prepared for each slide. TUNEL mix was composed of 95% labeling solution and five percent enzyme solution by volume. This mix was added to slides, which were incubated at 37˚C for one hour in a humidified container. Finally, slides were passed through three washes, first a three minute PBS wash, then a five minute 4',6-diamidino-2-phenylindole (DAPI) wash, and finally a three minute PBS wash. The DAPI wash consisted of a 1:10,000 dilution of DAPI in PBS. Following the third wash, slides were cover-slipped with n-propyl gallate used as the mounting agent. Slides were stored at four degrees Celsius before imaging.

Table 1: Chemical and Biological Reagents

Reagent Type	***Name***	***Distributor***	***Identifiers***	***Notes***
Antibody	Ki-67 Monoclonal Antibody (SolA15)	ThermoFischer Scientific	Cat. # 14-5698-82	1:100 dilution IHC-F (TW)
Antibody	Polyclonal Human LRIG1 Antibody (goat α LRIG1)	R&D Systems	Cat. # AF3688	1:500 dilution IHC-F (TLL)

Antibody	Non-phospho (Active) ß-Catenin (Ser45) (D2U8Y) XP® Rabbit mAb	Cell Signaling Technology	Cat. # 19807	1:750 dilution IHC-F
Antibody	Polyclonal Antibody to Mucin 2	CloudClone	Cat. # PAA705Mu01	1:100 dilution IHC-P
Antibody	Polyclonal Alexa Fluor® 488 AffiniPure Donkey α rabbit IgG	JacksonImmunoResearch	Cat. # 711-545-152	1:500 dilution IHC-F
Antibody	Polyclonal Alexa Fluor® 488 AffiniPure Donkey α rat IgG	JacksonImmunoResearch	Cat. # 712-545-150	1:500 dilution IHC-F
Antibody	Alexa Fluor® 488 Phalloidin	ThermoFisher Scientific	Cat. # A12379	1:2500 Dilution IHC-F
Antibody	Polyclonal Alexa Fluor® 647 AffiniPure Donkey α goat IgG	JacksonImmunoResearch	Cat. # 712-545-150	1:500 dilution IHC-F
Antibody	Polyclonal Cy3® (λ = 568nm) AffiniPure Donkey α Rabbit IgG	JacksonImmunoResearch	Cat. # 705-605-147	1:500 dilution IHC-F
Staining Kit	In Situ Cell Death Detection Kit	F. Hoffmann-La Roche AG	Cat. # 12156792910	Full kit used, contains many

				chemical reagents
Molecular Assay	Proteome Profiler Human Phospho-Kinase Array Kit	R & D Systems	Cat. # ARY003C	Assay used to detect expression of 37 kinases and 2 related proteins.
Model Organism	*C57BL/6*	Jackson Laboratory (Jax), Bar Harbor, ME	Strain #:000664	
Chemical Reagent	Dextran Sodium Sulfate	TdB labs	Batch # DB001-41	
Microscope	Nikon Eclipse/Ds-Ri2	Nikon, Tokyo, Japan	ID # Ni-SSR	
Biomolecular imager	Amersham Typhoon	GE Healthcare	Product # 29187191	
Cryostat	Leica 710 CM	Leica, Wetzlar, Germany	Product ID# CM1860	

Results

Homeostasis of the colonic epithelium relies upon self-renewal of crypts. To accomplish this, it must maintain a careful balance between proliferative and differentiated cells. During regeneration after an injury to the epithelium, this balance becomes even more critical, as an increase of proliferative cells will rapidly expand the epithelium. After this expansion, a wave of differentiation is required to generate the absorptive and secretory cells required for colon function. Together, these processes are regulated by many known molecular pathways, yet how the colon resets crypt function after an injury is still incompletely understood. The overall goal of my thesis was to carefully examine this injury-repair process in the presence and absence of an important protein, Leucine rich repeats and immunoglobulin-like domains-3 (Lrig3). My first step was to examine the extent of epithelial injury after acute inflammatory assault using 3% Dextran Sodium Sulfate (DSS) dissolved in the drinking water, on wildtype (*WT*) and *Lrig3*$^{-/-}$ mice. I treated the mice with DSS for six days, followed by 24 hours of normal water, extracted the colons, and stained colonic tissue sections with 4′,6-diamidino-2-phenylindole (DAPI) and β-catenin (Figure 1) to visualize the tissue and quantify the number of nuclei per crypt in each cohort (Figure 1). There were no gross morphological differences between genotypes. I quantified the number of epithelial cells remaining after DSS treatment by measuring the number nuclei per crypt from 10 images from 12 animals with equal representation of each genotype. There was no difference between cohorts (Figure 1B). We also compared these data with previous lab work, by comparing the number of cells per crypt in adult mice during homeostasis (Figure 1B “naïve” mice) and find *Lrig3*$^{-/-}$ mice had more nuclei per crypt than *WT*

mice. When comparing the number of cells per crypt remaining in inflammatory assault to the number of nuclei per crypt in homeostasis, we find significantly less nuclei in the *Lrig3*$^{-/-}$ cohort (Figure 1B, p<0.0001), but no change in *WT* mice (Figure 1B, p=0.0568). These data contrast our results in DSS indicating that *Lrig3*$^{-/-}$ mice have fewer nuclei per crypt than wildtype mice in recovery from acute inflammatory assault.

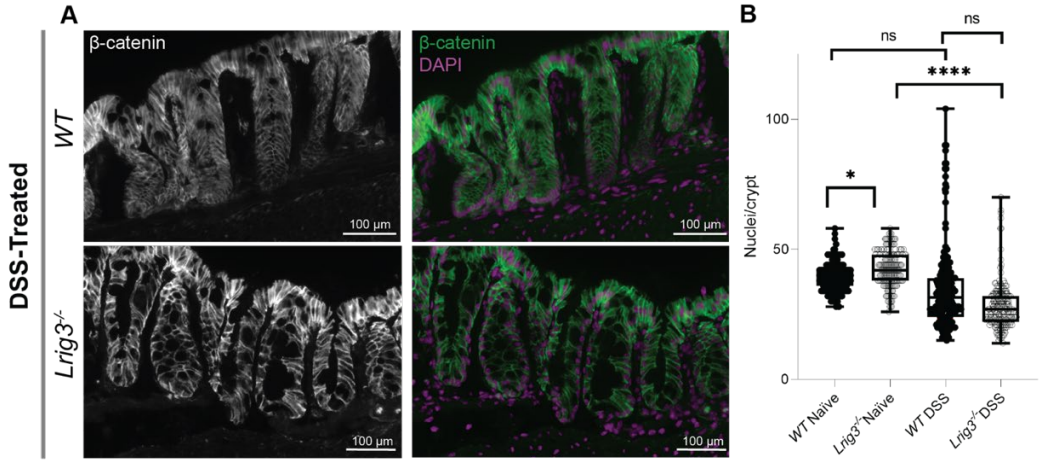

Figure 1: DSS treated *Lrig3*$^{-/-}$ mice have fewer nuclei per crypt than *WT* mice.

(A) Immunofluorescence stains with β-catenin in white on left panels and green on the right. DAPI marks nuclei in magenta on the right panels. (B) Quantification of nuclei per crypt reveals significantly fewer nuclei per crypt in mutant tissue after treatment when compared to mutant untreated tissue (p<0.0001), no significant difference between nuclei in *WT* treated and untreated tissue, and no significant difference between nuclei per crypt in *WT* treated and mutant treated tissue. n=6 mice/genotype.

DSS-treated Lrig3$^{-/-}$ *mice exhibit fewer proliferating cells than their WT counterparts.*

Given there was no change in the number of nuclei per crypt after DSS, we then examined the potential reasons why *Lrig3*$^{-/-}$ mice are unable to maintain the number of cells within their crypts after DSS treatment. One potential reason for this could be perturbed cell turnover, defined as the proliferation and maintenance of new cells. To

examine this, I used the proliferation marker Kiel-67 (Ki-67) and co-stained for nuclei (DAPI) to identify the crypt borders and assist in finding positive cells within colonic crypts. This approach allowed me to avoid the misidentification of leukocytes intercalated between regenerating crypts as epithelial cells. In Figure 2A, I show images from each genotype. These were morphologically different from each other, and proliferation appeared to be strictly confined to the crypt-base in the wildtype tissue and increased compared to *Lrig3*$^{-/-}$ mice. The number of Ki-67 positive cells per crypt was decreased in the mutant cohort (Figure 2B, p=0.0445). These results show a decreased amount of proliferation in *Lrig3*$^{-/-}$ mice after acute inflammatory assault when compared to wildtype.

TUNEL identifies more cells marked for programmed death in Lrig3$^{-/-}$ *mice.*

After identifying a decreased amount of proliferation in *Lrig3*$^{-/-}$ mice, I postulated that the fewer number of nuclei per crypt could be due to the lack of proliferation or an increase in cellular death. To investigate the latter possibility, I used a terminal deoxynucleotidyl transferase dUTP nick end labeling (TUNEL) assay to identify double stranded breaks in DNA as a result of apoptosis. Again, I used a DAPI co-stain to identify crypt borders and help provide positional data on where cell death is occurring. Figure 3A contains images of tissue from each genotype and there is not increased cell death in either genotype. The data, however, indicate more cell death in the *Lrig3*$^{-/-}$ cohort in the upper and lower portions of crypts compared to wildtype. Interestingly, I did not detect any differences between death in the crypt cuff (Figure 3B, p<0.01). Cell death is localized to particular regions of colon crypts in *Lrig3*$^{-/-}$ mice compared to *WT*.

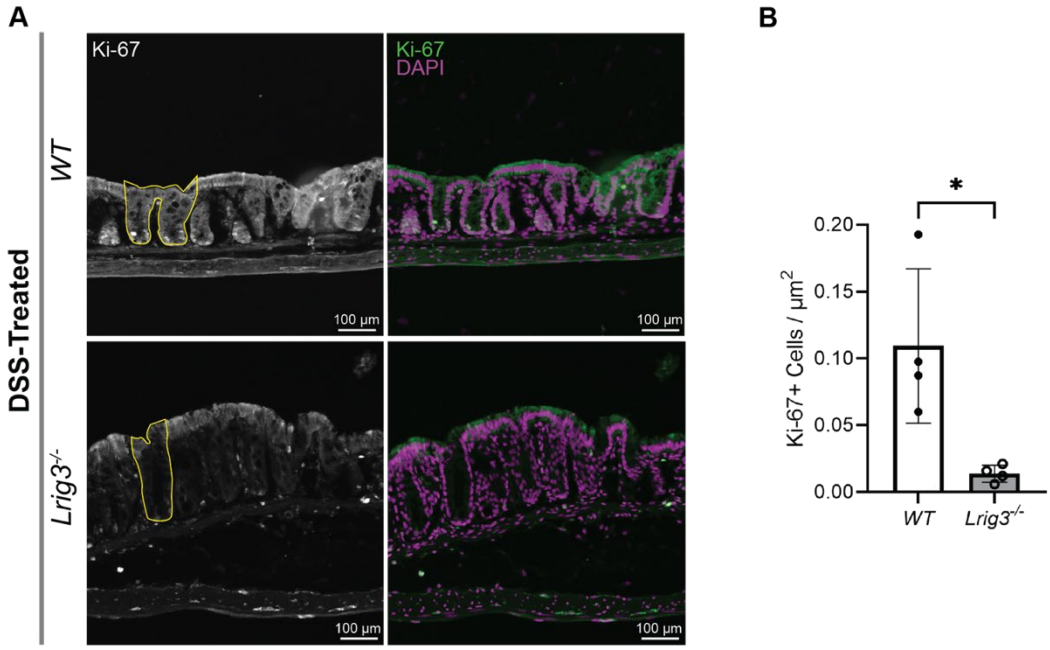

Figure 2: DSS treated *Lrig3*$^{-/-}$ mice have fewer proliferating cells than their *WT* counterparts.

(A) Immunofluorescence stains with Ki-67 in white on left panels and green on the right. DAPI is in magenta on the right and identifies all nuclei in the tissue. Yellow outlines epithelial area considered in analysis for these images. (B) Number of Ki-67+ cells per µm^2 (epithelial area). n=4 mice/genotype normalized to 1778 +/- 125µm^2, p=0.0445.

DSS treated Lrig3$^{-/-}$ mice exhibit lower expression of Lrig1 than their WT counterparts

As the *Lrig3*$^{-/-}$ mice had increased cell death and decreased proliferation after DSS-treatment, compared to *WT*, I reasoned the lack of proliferation could be resulting from a diminished stem cell population in *Lrig3*$^{-/-}$ mice. To examine this, I assessed the colonic epithelium for the presence of stem cells. As other stem cell markers are absent after DSS treatment, I chose to examine the tissue for the presence of Leucine rich repeats and immunoglobulin-like domains-1 (Lrig1)-expressing stem cells, as in prior lab experiments, expression of this stem cell marker was expanded in the recovery period from DSS treatment in *WT* mice. To accomplish this analysis, I identified nuclei with a DAPI co-stain, which allowed for easier quantification of the extent of Lrig1 expression by cells. I have two observations from my analyses. The first is a stark morphological contrast between genotypes with a near absence of Lrig1 expression in *Lrig3*$^{-/-}$ mice. The overall colonic expression of Lrig1 is reduced in *Lrig3*$^{-/-}$ mice when compared to *WT* (Figure 4B, $p<0.01$). It is clear that expression of this stem cell marker is severely diminished in *Lrig3*$^{-/-}$ mice when compared to *WT*, during the recovery period from acute inflammatory assault by DSS.

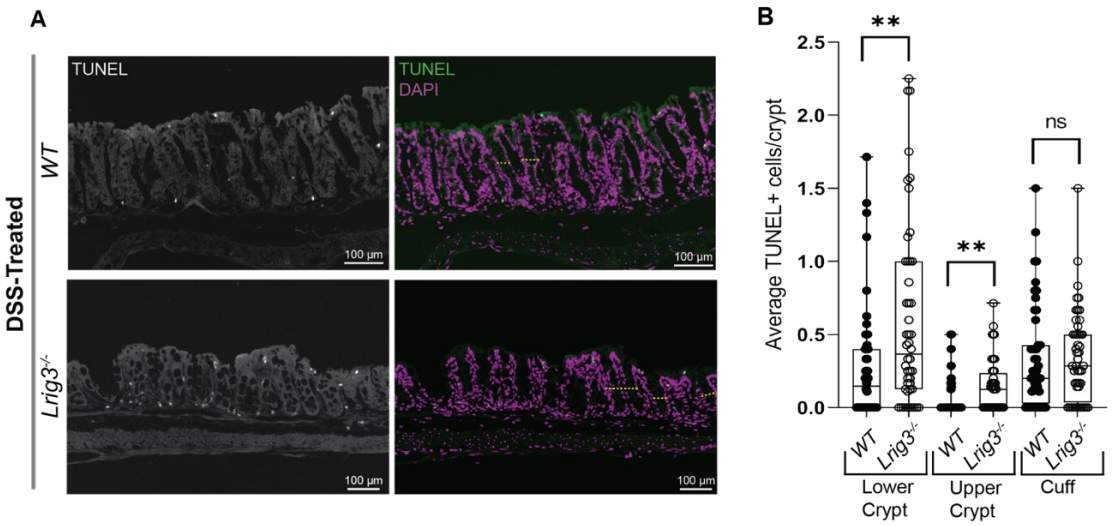

Figure 3: TUNEL identifies more cells marked for programmed death in *Lrig3*$^{-/-}$ mice.

(A) TUNEL assay with positive cells marked in white on the left and green on right panels. DAPI in magenta on left panels identifies nuclei. Yellow dashed lines indicate separation between upper and lower halves of crypts. (B) Quantification of average TUNEL positivity per crypt. n=6 mice/genotype, 128 crypts/genotype, $p<0.01$.

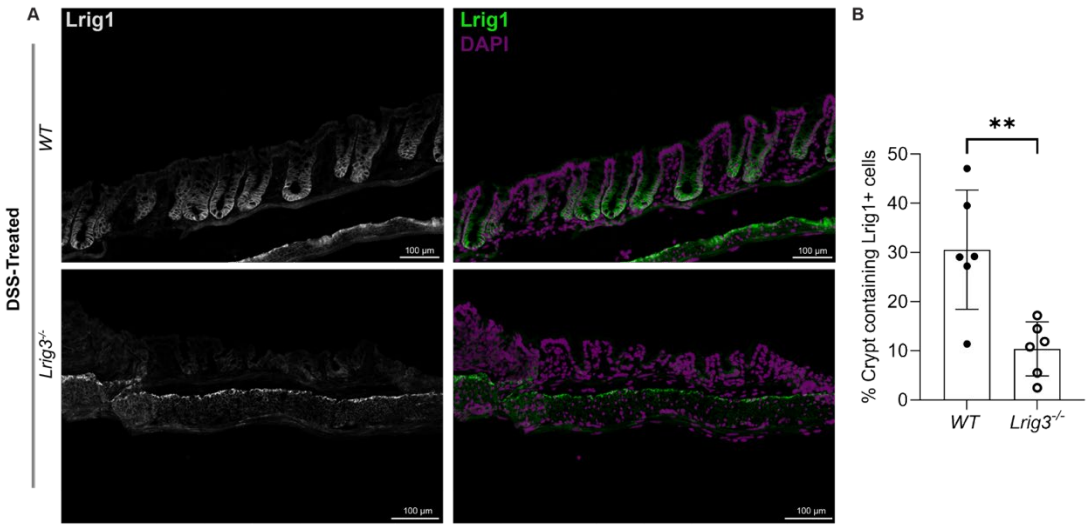

Figure 4: DSS treated *Lrig3*$^{-/-}$ mice exhibit lower expression of Lrig1 than their WT counterparts.

(A) Immunofluorescence staining with Lrig1 in white on the left panels and green on the right. DAPI in magenta on the left panels identifies all nuclei in the tissue. (B) Generated percentage of Lrig1 positivity calculated by measuring the height at which Lrig1 expression is highest in a crypt and taking the percentage of that over the total height of the intact crypt. $p<0.01$, n=6 mice/genotype.

Regulation of differentiated cells is unchanged in Lrig3$^{-/-}$ mice after acute inflammatory assault.

My data thus far indicate that there is a perturbed stem cell niche in *Lrig3*$^{-/-}$ mice consisting of fewer stem cells, less proliferation, and increased cell death compared to wildtype cohorts. Given these disruptions, I investigated the existence of the differentiated cell population by examining the tissue for cell-specific markers of differentiation. The first marker I examined to ascertain the robustness of the differentiated population was Mucin2 (Muc2). Muc2 is produced by secretory colonic epithelial cells and identifies the mucus-rich lining of the epithelial tissue. To analyze the mucus production in the colonic epithelium, I examined Muc2 expression alongside DAPI as a co-stain to delineate crypt borders, as I had done previously. After analyzing tissue from both cohorts, I observe no appreciable difference between genotypes in terms of mean percentage Muc2 expression area over luminal area (Figure 5A, B). The second marker I examined to ascertain the robustness of the differentiated population was phalloidin, also known as F-actin. In my knockout and control mice, I examined F-actin expression by detection of phalloidin and used DAPI co-stain to demarcate individual nuclei and crypt borders. Empirically, there are no differences across genotype in phalloidin binding (Figure 6). Taken together, the preserved expression of Muc2 and F-actin suggests the differentiated portion of colonic crypts is intact in *Lrig3*$^{-/-}$ and control mice after DSS treatment.

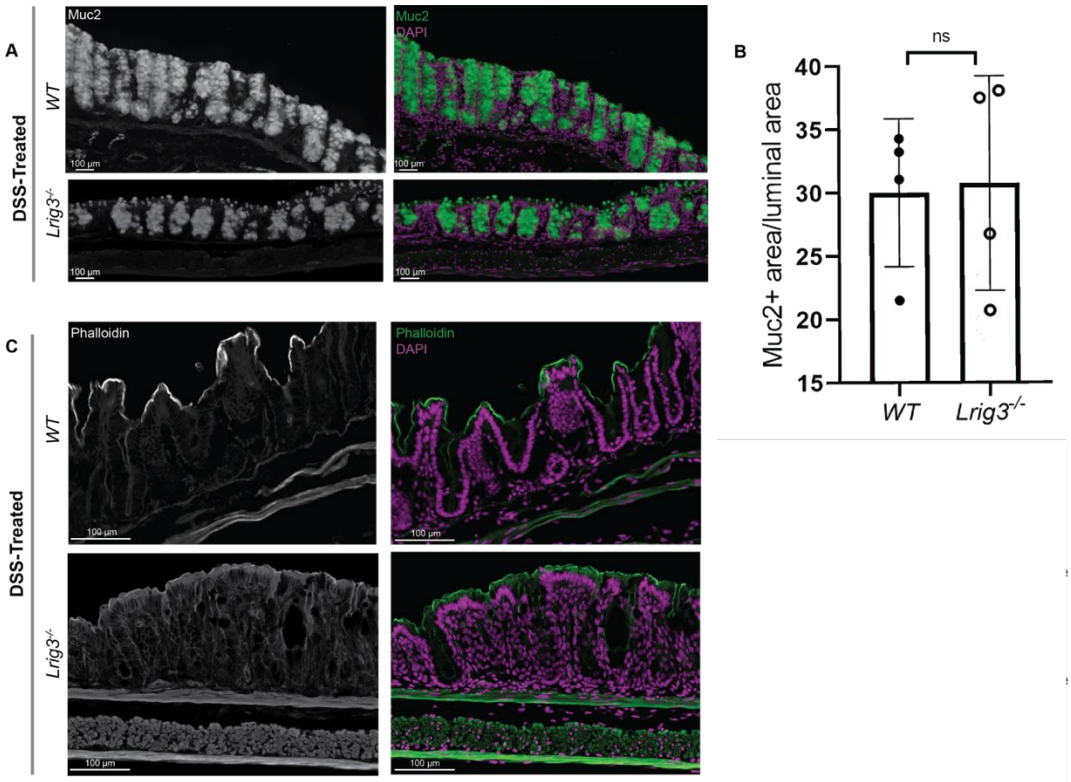

Figure 5: Regulation of differentiated cells is unchanged in *Lrig3*$^{-/-}$ mice after acute inflammatory assault.

(A) Immunofluorescence stains with Muc2 in white on the left panels and green on the right. DAPI marks nuclei in magenta on the right panels. (B) Quantification of Muc2 expressed area over the total crypt area reveals no appreciable differences, n=4 mice/genotype, p=0.445. (C) Phalloidin expression as detected by phalloidin antibody in white on the left panels and green on the right. DAPI marks nuclei in magenta.

Receptor kinase signaling is unchanged in DSS-treated Lrig3$^{-/-}$ mice

In addition to examining the mice for differentiated cells, I thought it reasonable to assess signaling pathways that contribute directly to determining cell types as these might serve as the basis for the decreased proliferation and increased cell death, which I observed in my *Lrig3*$^{-/-}$ mice. To achieve this, I took a global array-based approach by using a receptor tyrosine kinase (RTK) array kit to interrogate the expression of 39 proteins simultaneously. This chemiluminescence-based immunoassay detects specific proteins present in an extract prepared from each mouse colon. Specifically, it detects the presence of the phosphorylated (activated) forms of specific proteins. Two proteins of interest I was examined were Epidermal Growth Factor Receptor (pEGFR) and Ras-dependent extracellular signal-regulated kinase (pERK1/2). EGFR is known to act protectively against apoptosis in intestinal inflammation (Yamaoka et al., 2008) and ERK1/2 is a kinase that is activated during cellular proliferation (Niederlechner et al., 2013). Given the increase in apoptosis in *Lrig3*$^{-/-}$ mice, I hypothesized I would observe a decrease in pEGFR in the protein lysates from the *Lrig3*$^{-/-}$ colon tissue, compared to *WT* mice. Similarly, I also expected to observe a decrease in pERK1/2, given the observed lack of proliferation in *Lrig3*$^{-/-}$ compared to *WT* mice. After comparing expression of these proteins in the protein extracts from both cohorts of mice, I did not detect any differences across genotypes (Figure 6). In conclusion, these signaling axes are unchanged in the mice at this timepoint.

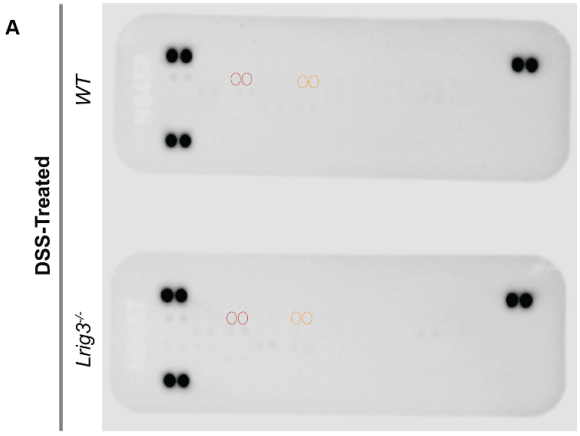

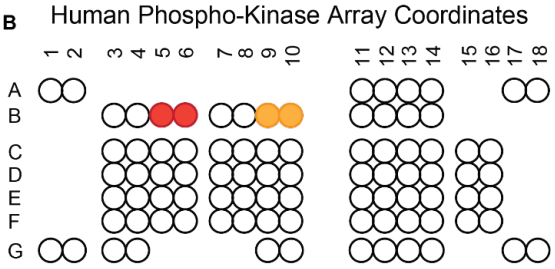

Membrane/ Coordinate	Target/Control	Membrane/ Coordinate	Target/Control
A-A1, A2	Reference Spot	A-E3, E4	p38α
B-A11, A12	Akt 1/2/3	A-E5, E6	PDGF Rβ
B-A13, A14	Akt 1/2/3	A-E7, E8	PLC-γ1
B-A17, A18	Reference Spot	A-E9, E10	Src
A-B3, B4	CREB	B-E11, E12	PYK2
A-B5, B6	EGF R	B-E13, E14	RSK1/2
A-B7, B8	eNOS	B-E15, E16	RSK1/2/3
A-B9, B10	ERK1/2	A-F3, F4	STAT2
B-B11, B12	Chk-2	A-F5, F6	STAT5a/b
B-B13, B14	c-Jun	A-F7, F8	WNK1
A-C3, C4	Fgr	A-F9, F10	Yes
A-C5, C6	GSK-3α/β	B-F11, F12	STAT1
A-C7, C8	GSK-3β	B-F13, F14	STAT3
A-C9, C10	HSP27	B-F15, F16	STAT3
B-C11, C12	p53	A-G1, G2	Reference Spot
B-C13, C14	p53	A-G3, G4	β-Catenin
B-C15, C16	p53	A-G9, G10	PBS (Negative Control)
A-D3, D4	JNK 1/2/3	B-G11, G12	STAT6
A-D5, D6	Lck	B-G13, G14	HSP60
A-D7, D8	Lyn	B-G17, G18	PBS (Negative Control)
A-D9, D10	MSK1/2		
B-D11, D12	p70 S6 Kinase		
B-D13, D14	p70 S6 Kinase		
B-D15, D16	PRAS40		

Figure 6: Receptor kinase signaling is unchanged in *Lrig3*$^{-/-}$ mice compared to *WT* mice.

(A) Receptor Tyrosine Kinase (RTK) assay with blots for 39 kinases. *WT* is the upper gel, *Lrig3*$^{-/-}$lower gel. Images show no gross differences across genotypes. Red and yellow circles mark proteins associated with the EGFR pathway. n=3 mice/genotype. (B) Key for reading RTK gels adapted from R&D systems RTK product datasheet, catalogue number: ARY001B.

Discussion

The colon is a highly regulated organ with a specific structure that affords its function. In this structure are small, U-shaped invaginations in the epithelium called crypts. These crypts are responsible for maintaining the functions of the colon, secreting protective mucous and absorbing water. One gene with expression throughout the colonic crypt is *Leucine-rich repeats and immunoglobulin-like domains 3 (Lrig3)* which may be crucial in regulating the size and structure of the stem cell region in these crypts. Previous data indicate the stem cell niche is perturbed in homeostasis when this gene is knocked out of the genome, but it is unclear if these perturbations impact the ability of loss-of-function (*Lrig3*$^{-/-}$) mice to regenerate from acute inflammatory assault. To assess the ability of *Lrig3*$^{-/-}$ mice to respond to inflammatory injury, we administered 3% Dextran Sodium Sulfate (DSS) to wildtype (*WT*) mice and *Lrig3*$^{-/-}$ mice for six days and allowed 24 hours of recovery on untreated drinking water. In this treatment period, we observed increased weight loss and increased colon shortening in our *Lrig3*$^{-/-}$ cohort indicating a possibly impaired regenerative response to the insult (Eichele & Kharbanda, 2017). To assess this, we examined the *Lrig3*$^{-/-}$ and *WT* colon tissue for the presence of intact cells, and molecular markers of stem cells, differentiate cellular lineages, as well as indicators of sustained proliferation and cell death. Our analysis indicated the *Lrig3*$^{-/-}$ mice lack intact stem cells and have decreased proliferation. These phenotypes are accompanied by an increase in cell death. Interestingly, the differentiated population of epithelial colon crypts does not appear impaired. Taken together, our data indicate the regenerative response after acute epithelial injury is impaired in *Lrig3*$^{-/-}$ mice, compared to the *WT* cohort.

The colon will start to rebuild itself almost immediately after injury through an expansion of the residual epithelium (Meyer et al., 2022) and this process is critical for the life of the organ. As our *Lrig3*$^{-/-}$ mice struggled to survive the acute inflammatory assault, the first thing we wanted to do was take a cellular census to examine the amount of epithelium that remained after the injury. To accomplish this, we examined the number of epithelial nuclei remaining in crypts, also known as 'crypt depth', after DSS treatment, yet we did not detect any differences in the number of nuclei when comparing *WT* and *Lrig3*$^{-/-}$ mice after this acute inflammatory assault. These results are particularly striking when compared to similar measures taken by our lab in homeostasis, which indicate that have significantly greater crypt depth than their *WT* counterparts. In short, it seems the *Lrig3*$^{-/-}$ mice cannot either maintain or recover this increase crypt depth. The loss of this relative relationship after DSS suggests a greater extent of epithelial injury in our *Lrig3*$^{-/-}$ mice. As our data show greater weight loss and colon shortening in *Lrig3*$^{-/-}$ mice we hypothesize that these physiological impacts may be a direct result of this loss of crypt depth. This would be important to look at in future studies. In addition, it will be important to examine the tissue in the days while the mice are subjected to DSS, rather than after the DSS treatment is completed to develop a more comprehensive picture of how quickly this deficit develops.

As the epithelium was not regenerative after DSS treatment and this resulted in a loss of crypt depth, we hypothesized this was due to one of two deficiencies: a lack of proliferation or an increase in cellular death. Our first step was to evaluate an indicator of sustained proliferation, Kiel-67 (Ki-67), which is known to be elevated in *WT* mice following DSS-induced colitis (Wang et al., 2019). Our analysis shows fewer

proliferating cells per area in our *Lrig3*$^{-/-}$ mice, compared to *WT* controls. These data support our previous results with the number of nuclei remaining per crypt and provide a basis for the inability of mice to regenerate following acute inflammatory injury. In short, *Lrig3*$^{-/-}$ mice seemingly are unable to rapidly generate new cells once the inflammatory injury has taken place. Taken together with our nuclei data, we formulate the hypothesis that *Lrig3*$^{-/-}$ mice have a deficit in the production of new cells in the regenerative period of DSS-mediated colitis which leads to an inability to fully recover crypt depth. Future studies focusing on determining when this deficit arises during the inflammatory period, and if it can self-correct during recovery on normal water will be important to help us understand the molecular mechanism behind this lack of regeneration. These studies would be enhanced by using an approach to visualize the cell cycle, such as the incorporation of 5-ethynyl-2'-deoxyuridine, to understand which cells are stopping the cell cycle over a time course.

After identifying a deficit in one of the two possible branches for an explanation of the relative loss of crypt depth in *Lrig3*$^{-/-}$ mice compared to *WT* controls, we were eager to investigate whether excess cell death was also present in our tissue, which would also restrict crypt depth. Cellular death is a hallmark epithelial response to DSS treatment (da Silva et al., 2006) and contributes to the process of epithelial ulceration. Using terminal deoxynucleotidyl transferase dUTP nick end labeling (TUNEL) we discovered more cell death in loss-of-function mice when compared to *WT* controls, with most of the death occurring within the crypt cuff (the top of the crypts) but not within crypt walls. Cuff cells normally slough off and this process is increased after DSS, yet it seems our *Lrig3*$^{-/-}$ mice have increased death in the cuff (Okumura &

Takeda, 2017). While this is an interesting observation, death in the cuff region should not restrict the crypt depth, so it seems that these data do not impact the loss of crypt depth that we observe. In the future, it will be important to examine the source of this excess cell death in the cuff region, perhaps using time course-based studies. in the initial injury period with DSS to develop a clearer picture of when cell death occurs in this dynamic process.

With a lack of sustained proliferation identified in our loss-of-function model, we hypothesized that the reserve stem cell population had been damaged or was unable to enter the cell cycle thus leading to the lack of proliferation. In the acute model of inflammatory assault, the resident active stem cells of the colonic epithelium, Leucine-rich repeat-containing G-protein coupled receptor 5 positive (Lgr5+) cells, are ablated (Davidson et al., 2012). This places part of the regenerative burden on the reserve stem cell population of which Lrig1+ cells are known to respond to injury by proliferating and rebuilding the niche (Powell et al., 2012). Our analysis of Lrig1 in our tissue reveals a nearly absent reserve stem cell population at the 24-hour recovery timepoint in our *Lrig3*$^{-/-}$ cohort when compared to *WT* controls. These data further support our hypothesis that *Lrig3*$^{-/-}$ mice have a deficit in the production of new cells during the regenerative period of acute inflammatory assault. The significantly perturbed reserve stem cell population is compelling evidence but could be strengthened further by investigating other reserve stem cell markers such as B lymphoma Mo-MLV insertion region 1 homolog (Bmi1) which is an intestinal reserve stem cell marker that also responds to injury but is rarely seen in the colon (Yan et al., 2012). A second marker of reserve stem cells, mouse telomerase reverse transcriptase (mTert), could be

contributing to the regenerative response (Montgomery et al., 2011) but the lack of proliferation in our tissue lowers the index of suspicion for this possibility.

So far, our data describe a stem cell niche that can achieve and maintain homeostasis but cannot mount a regenerative response once an inflammatory insult occurs. To this point, I have not discussed the differentiated cell populations which are responsible for carrying out the physiological functions of the colon. In addition, one of classic failures of differentiated cells after an injury process in the colon is the maintenance of tight epithelial barrier and continued expression of mucus to line the colon (Okumura & Takeda, 2017). Using a marker for Mucin-2 (Muc2) I did not identify any discrepancies in the expression of this protein across my experimental and control mice. Given this, it seems the stem cell niche is failing but this is not immediately impacting the behavior of the mucus-secreting cells. In addition to secreting mucus, the colonic epithelium must be capable of absorbing nutrients through absorptive cells. Again, I surveyed the expression of phalloidin, which marks absorptive cells, and I did not detect any differences across our cohorts. Together, these results suggest the differentiated population in *Lrig3*$^{-/-}$ colonic crypts is not impaired by the loss of the stem cells at this timepoint after acute inflammatory injury.

Given the aberrant maintenance of the stem cell niche in acute inflammatory assault, I wanted to compare the cell signalling profiles between the experimental and control mice. I hypothesized that aberrant cell signaling might contributing to the loss-of-stem-cell phenotype. Signaling molecules substantially contribute to cellular fate and interruptions in signaling pathways can lead to various disease states (Perrimon et al., 2012). To investigate a subset of signaling proteins called receptor tyrosine kinases, we

employed an array-based assay screening for many pathways, including the proliferative WNT pathway, which is known to regulate colon stem cells (Mah et al., 2016). I did not detect any significant difference in activated cell signaling between the experimental and control mice of mice using this assay. This indicated there was no change in signalling at our selected timepoint. However, it is important to note that the selected time point is a very narrow timeframe in a much larger injury and recovery time course and this one timepoint cannot describe the dynamicity of signals in these mice throughout the DSS time course. A pertinent next step would be to investigate the expression profile of these proteins 24 hours after starting DSS administration and on each subsequent day during the inflammatory process to uncover the dysregulation resulting in the phenotype we observe in *Lrig3*$^{-/-}$ mice.

In conclusion, the aim of my study was to test the hypothesis that loss of *Lrig3* impairs colonic regeneration after acute inflammatory assault. I show *Lrig3*$^{-/-}$ mice display a higher susceptibility to DSS treatment than *WT* as supported by greater weight loss and increased colon shortening. Compared to *WT* mice, *Lrig3*$^{-/-}$ mice expressed lower levels proliferation and greater levels of cell death. *Lrig3*$^{-/-}$ mice fail to maintain or regenerate their stem cells after DSS treatment, in contrast to *WT* mice. Despite this, markers of both secretory and absorptive epithelial cell lineages, as well as key receptor kinase signaling pathways, were unchanged. Together, my study determined that loss of *Lrig3* significantly impairs colonic regeneration after acute inflammatory assault. While the role of *Lrig3* in colon homeostasis is still under investigation, Lrig3 protein plays a key role in colonic regeneration after injury.

Bibliography

Abraira, V. E., Satoh, T., Fekete, D. M., & Goodrich, L. V. (2010). Vertebrate Lrig3-ErbB Interactions Occur In Vitro but Are Unlikely to Play a Role in Lrig3-Dependent Inner Ear Morphogenesis. *PLoS ONE*, *5*(2), e8981. https://doi.org/10.1371/journal.pone.0008981

Aslam, N., Lo, S. W., Sikafi, R., Barnes, T., Segal, J., Smith, P. J., & Limdi, J. K. (2022). A review of the therapeutic management of ulcerative colitis. *Therapeutic Advances in Gastroenterology*, *15*, 175628482211381. https://doi.org/10.1177/17562848221138160

Biressi, S., Chiacchiera, F., Okamoto, R., Steiner, T. S., Rees, W. D., Tandun, R., Yau, E., & Zachos, N. C. (2020). *Regenerative Intestinal Stem Cells Induced by Acute and Chronic Injury: The Saving Grace of the Epithelium?* https://doi.org/10.3389/fcell.2020.583919

Boye, T. L., Steenholdt, C., Jensen, K. B., & Nielsen, O. H. (2022). Molecular manipulations and intestinal stem cell-derived organoids in inflammatory bowel disease. *Stem Cells*, sxac014. https://doi.org/10.1093/stmcls/sxac014

Coskun, M., Salem, M., Pedersen, J., & Nielsen, O. H. (2013). Involvement of JAK/STAT signaling in the pathogenesis of inflammatory bowel disease. *Pharmacological Research*, *76*, 1–8. https://doi.org/10.1016/j.phrs.2013.06.007

da Silva, A. P. B., Pollett, A., Rittling, S. R., Denhardt, D. T., Sodek, J., & Zohar, R. (2006). Exacerbated tissue destruction in DSS-induced acute colitis of OPN-null mice is associated with downregulation of TNF-α expression and non-programmed cell death. *Journal of Cellular Physiology*, *208*(3), 629–639. https://doi.org/10.1002/jcp.20701

Davidson, L. A., Goldsby, J. S., Callaway, E. S., Shah, M. S., Barker, N., & Chapkin, R. S. (2012). Alteration of colonic stem cell gene signatures during the regenerative response to injury. *Biochimica et Biophysica Acta*, *1822*(10), 1600. https://doi.org/10.1016/J.BBADIS.2012.06.011

De Simone, B., Davies, J., Chouillard, E., Di Saverio, S., Hoentjen, F., Tarasconi, A., Sartelli, M., Biffl, W. L., Ansaloni, L., Coccolini, F., Chiarugi, M., De'Angelis, N., Moore, E. E., Kluger, Y., Abu-Zidan, F., Sakakushev, B., Coimbra, R., Celentano, V., Wani, I., … Catena, F. (2021). WSES-AAST guidelines: management of inflammatory bowel disease in the emergency setting. *World Journal of Emergency Surgery*, *16*(1), 23. https://doi.org/10.1186/s13017-021-00362-3

del Rio, T., Nishitani, A. M., Yu, W. M., & Goodrich, L. V. (2013). In Vivo Analysis of Lrig Genes Reveals Redundant and Independent Functions in

the Inner Ear. *PLOS Genetics*, *9*(9), e1003824. https://doi.org/10.1371/JOURNAL.PGEN.1003824

Dufourt, G., Demers, M. J., Gagné, D., Dydensborg, A. B., Teller, I. C., Bouchard, V., Degongre, I., Beaulieu, J. F., Cheng, J. Q., Fujita, N., Tsuruo, T., Vallée, K., & Vachon, P. H. (2004). Human Intestinal Epithelial Cell Survival and Anoikis: DIFFERENTIATION STATE-DISTINCT REGULATION AND ROLES OF PROTEIN KINASE B/Akt ISOFORMS *. *Journal of Biological Chemistry*, *279*(42), 44113–44122. https://doi.org/10.1074/JBC.M405323200

Eichele, D. D., & Kharbanda, K. K. (2017). Dextran sodium sulfate colitis murine model: An indispensable tool for advancing our understanding of inflammatory bowel diseases pathogenesis. *World Journal of Gastroenterology*, *23*(33), 6016–6029. https://doi.org/10.3748/WJG.V23.I33.6016

Gehart, H., & Clevers, H. (2018). Tales from the crypt: new insights into intestinal stem cells. *Nature Reviews Gastroenterology & Hepatology 2018 16:1*, *16*(1), 19–34. https://doi.org/10.1038/s41575-018-0081-y

Gordon Betts, J., Young, K. A., Wise, J. A., Johnson, E., Poe, B., Kruse, D. H., Korol, O., Johnson, J. E., Womble, M., & DeSaix, P. (2022). *Anatomy and Physiology 2e* (2e ed.). Openstax.

Guo, D., Yang, H., Guo, Y., Xiao, Q., Mao, F., Tan, Y., Wan, X., Wang, B., & Lei, T. (2015). LRIG3 modulates proliferation, apoptosis and invasion of glioblastoma cells as a potent tumor suppressor. *Journal of the Neurological Sciences*, *350*(1–2), 61–68. https://doi.org/10.1016/J.JNS.2015.02.015

Kappelman, M. D., Moore, K. R., Allen, J. K., & Cook, S. F. (2013). Recent trends in the prevalence of Crohn's disease and ulcerative colitis in a commercially insured US population. *Digestive Diseases and Sciences*, *58*(2), 519–525. https://doi.org/10.1007/S10620-012-2371-5

Lee, J. M., & Lee, K.-M. (2016). Endoscopic Diagnosis and Differentiation of Inflammatory Bowel Disease. *Clinical Endoscopy*, *49*(4), 370–375. https://doi.org/10.5946/ce.2016.090

Mah, A. T., Yan, K. S., & Kuo, C. J. (2016). Wnt pathway regulation of intestinal stem cells. *The Journal of Physiology*, *594*(17), 4837–4847. https://doi.org/10.1113/JP271754

Meyer, A. R., Brown, M. E., McGrath, P. S., & Dempsey, P. J. (2022). Injury-Induced Cellular Plasticity Drives Intestinal Regeneration. *Cellular and Molecular Gastroenterology and Hepatology*, *13*(3), 843–856. https://doi.org/10.1016/j.jcmgh.2021.12.005

Mikocka-Walus, A., Knowles, S. R., Keefer, L., & Graff, L. (2016). Controversies Revisited: A Systematic Review of the Comorbidity of Depression and Anxiety with Inflammatory Bowel Diseases. *Inflammatory Bowel Diseases*, *22*(3), 752–762. https://doi.org/10.1097/MIB.0000000000000620

Montgomery, R. K., Carlone, D. L., Richmond, C. A., Farilla, L., Kranendonk, M. E. G., Henderson, D. E., Baffour-Awuah, N. Y., Ambruzs, D. M., Fogli, L. K., Algra, S., & Breault, D. T. (2011). Mouse telomerase reverse transcriptase (mTert) expression marks slowly cycling intestinal stem cells. *Proceedings of the National Academy of Sciences*, *108*(1), 179–184. https://doi.org/10.1073/pnas.1013004108

Niederlechner, S., Baird, C., Petrie, B., Wischmeyer, E., & Wischmeyer, P. E. (2013). Epidermal growth factor receptor expression and signaling are essential in glutamine's cytoprotective mechanism in heat-stressed intestinal epithelial-6 cells. *American Journal of Physiology-Gastrointestinal and Liver Physiology*, *304*(5), G543–G552. https://doi.org/10.1152/ajpgi.00418.2012

Okumura, R., & Takeda, K. (2017). Roles of intestinal epithelial cells in the maintenance of gut homeostasis. *Experimental & Molecular Medicine*, *49*(5), e338–e338. https://doi.org/10.1038/emm.2017.20

Pérez, L. M., de Lucas, B., & Gálvez, B. G. (2018). Unhealthy Stem Cells: When Health Conditions Upset Stem Cell Properties. *Cellular Physiology and Biochemistry*, *46*(5), 1999–2016. https://doi.org/10.1159/000489440

Perrimon, N., Pitsouli, C., & Shilo, B.-Z. (2012). Signaling Mechanisms Controlling Cell Fate and Embryonic Patterning. *Cold Spring Harbor Perspectives in Biology*, *4*(8), a005975–a005975. https://doi.org/10.1101/cshperspect.a005975

Powell, A. E., Wang, Y., Li, Y., Poulin, E. J., Means, A. L., Washington, M. K., Higginbotham, J. N., Juchheim, A., Prasad, N., Levy, S. E., Guo, Y., Shyr, Y., Aronow, B. J., Haigis, K. M., Franklin, J. L., & Coffey, R. J. (2012). The pan-ErbB negative regulator Lrig1 is an intestinal stem cell marker that functions as a tumor suppressor. *Cell*, *149*(1), 146–158. https://doi.org/10.1016/J.CELL.2012.02.042

Pulley, J., Todd, A., Flatley, C., & Begun, J. (2020). Malnutrition and quality of life among adult inflammatory bowel disease patients. *JGH Open*, *4*(3), 454–460. https://doi.org/10.1002/jgh3.12278

Qin, X. (2012). Etiology of inflammatory bowel disease: A unified hypothesis. *World J Gastroenterol*, *18*(15), 1708–1722. https://doi.org/10.3748/wjg.v18.i15.1708

Rafidi, H., Mercado, F., Astudillo, M., Fry, W. H. D., Saldana, M., Carraway, K. L., & Sweeney, C. (2013). Leucine-rich Repeat and Immunoglobulin Domain-containing Protein-1 (Lrig1) Negative Regulatory Action toward ErbB Receptor Tyrosine Kinases Is Opposed by Leucine-rich Repeat and Immunoglobulin Domain-containing Protein 3 (Lrig3). *Journal of Biological Chemistry*, *288*(30), 21593–21605. https://doi.org/10.1074/JBC.M113.486050

Rawla, P., Sunkara, T., & Barsouk, A. (2019). Epidemiology of colorectal cancer: incidence, mortality, survival, and risk factors. *Gastroenterology Review*, *14*(2), 89–103. https://doi.org/10.5114/pg.2018.81072

Sasaki, N., Sachs, N., Wiebrands, K., Ellenbroek, S. I. J., Fumagalli, A., Lyubimova, A., Begthel, H., Van Born, M. Den, Van Es, J. H., Karthaus, W. R., Li, V. S. W., López-Iglesias, C., Peters, P. J., Van Rheenen, J., Van Oudenaarden, A., & Clevers, H. (2016). Reg4+ deep crypt secretory cells function as epithelial niche for Lgr5+ stem cells in colon. *Proceedings of the National Academy of Sciences of the United States of America*, *113*(37), E5399–E5407. https://doi.org/10.1073/PNAS.1607327113/SUPPL_FILE/PNAS.201607327SI.PDF

Seyedian, S. S., Nokhostin, F., & Malamir, M. D. (2019). A review of the diagnosis, prevention, and treatment methods of inflammatory bowel disease. *Journal of Medicine and Life*, *12*(2), 113–122. https://doi.org/10.25122/jml-2018-0075

Simion, C., Cedano-Prieto, M. E., & Sweeney, C. (2014). The LRIG family: enigmatic regulators of growth factor receptor signaling. *Endocrine-Related Cancer*, *21*(6), R431–R443. https://doi.org/10.1530/ERC-14-0179

Sugimoto, S., Ohta, Y., Fujii, M., Matano, M., Shimokawa, M., Nanki, K., Date, S., Nishikori, S., Nakazato, Y., Nakamura, T., Kanai, T., & Sato, T. (2018). Reconstruction of the Human Colon Epithelium In Vivo. *Cell Stem Cell*, *22*(2), 171-176.e5. https://doi.org/10.1016/J.STEM.2017.11.012

Vancamelbeke, M., & Vermeire, S. (2017). The intestinal barrier: a fundamental role in health and disease. *Expert Review of Gastroenterology & Hepatology*, *11*(9), 821–834. https://doi.org/10.1080/17474124.2017.1343143

Wang, K., Zhan, X., McAlpine, W., Zhang, Z., Choi, J. H., Shi, H., Misawa, T., Yue, T., Zhang, D., Wang, Y., Ludwig, S., Russell, J., Tang, M., Li, X., Murray, A. R., Moresco, E. M. Y., Turer, E. E., & Beutler, B. (2019). Enhanced susceptibility to chemically induced colitis caused by excessive endosomal TLR signaling in LRBA-deficient mice. *Proceedings of the*

National Academy of Sciences, *116*(23), 11380–11389. https://doi.org/10.1073/pnas.1901407116

Worley, G., Almoudaris, A., Bassett, P., Segal, J., Akbar, A., Ghosh, S., Aylin, P., & Faiz, O. (2021). Colectomy rates for ulcerative colitis in England 2003-2016. *Alimentary Pharmacology & Therapeutics*, *53*(4), 484–498. https://doi.org/10.1111/apt.16202

Wray, N. R., Lin, T., Austin, J., McGrath, J. J., Hickie, I. B., Murray, G. K., & Visscher, P. M. (2021). From Basic Science to Clinical Application of Polygenic Risk Scores: A Primer. *JAMA Psychiatry*, *78*(1), 101–109. https://doi.org/10.1001/jamapsychiatry.2020.3049

Yamaoka, T., Yan, F., Cao, H., Hobbs, S. S., Dise, R. S., Tong, W., & Polk, D. B. (2008). Transactivation of EGF receptor and ErbB2 protects intestinal epithelial cells from TNF-induced apoptosis. *Proceedings of the National Academy of Sciences*, *105*(33), 11772–11777. https://doi.org/10.1073/pnas.0801463105

Yan, K. S., Chia, L. A., Li, X., Ootani, A., Su, J., Lee, J. Y., Su, N., Luo, Y., Heilshorn, S. C., Amieva, M. R., Sangiorgi, E., Capecchi, M. R., & Kuo, C. J. (2012). The intestinal stem cell markers Bmi1 and Lgr5 identify two functionally distinct populations. *Proceedings of the National Academy of Sciences*, *109*(2), 466–471. https://doi.org/10.1073/pnas.1118857109

Zhao, H., Tanegashima, K., Ro, H., & Dawid, I. B. (2008). Lrig3 regulates neural crest formation in *Xenopus* by modulating Fgf and Wnt signaling pathways. *Development*, *135*(7), 1283–1293. https://doi.org/10.1242/dev.015073